

Fabrication of a biocompatible flexible electroosmosis micropump

Amir Jahanshahi · Fabrice Axisa · Jan Vanfleteren

Received: 31 July 2011 / Accepted: 18 September 2011 / Published online: 6 December 2011
© Springer-Verlag 2011

Abstract In in-vivo microsystems, one of the components is a biocompatible micropump in order to produce the necessary force to deliver the fluid from the inlet to the outlet. In this contribution, a flexible micropump is fabricated which is aimed to be suitable in drug delivery applications. It provides high degree of biocompatibility, since the only employed materials are implantation grade polydimethylsiloxane elastomer and gold for the electrical interconnects. The working principle of the micropump is based on transverse DC electroosmosis which is a new variant of conventionally applied high voltage DC electroosmosis. This new technique is based on topography irregularities introduced in the channel resulting in a non-uniform charge distribution. The advantage is to drive the micropump using a relatively low DC voltage of 10 V while getting an effective flow speed of 60 $\mu\text{m/s}$. In order to characterize the flow speed, dyed 3 μm beads are dispersed in the working fluid and their speed is measured by the line scanning technique using a confocal microscope. It is also observed that the flow has a helical profile which is an attractive feature for an efficient micro-mixer in active microfluidics and μ -TAS applications.

Keywords PDMS · Micropump · Implantation · Osmosis

1 Introduction

For drug delivery and μ -TAS (micro total analysis systems), micropumps are always a necessary and at the same time challenging component because of the demanding requirements. These micropumps are driven using different actuating principles such as piezoelectric (van Lintel et al. 1988; Feng and Kim 2004), thermopneumatic (Kim et al. 2005; Jeong et al. 2005), electrostatic (Zengerle et al. 1995), and electrokinetic (Peterman et al. 2004; Chung et al. 2008). Comprehensive overviews of available technologies are available in the literature (Laser and Santiago 2004; Amirouche et al. 2009). In this work, the actuation principle and the material selection is discussed, in view of the requirements and restrictions imposed by the working environment of the final device.

The ultimate goal is the fabrication of a large area implantable drug delivery system, for which the pump presented here would eventually become one of the building blocks. The major requirements are not only biocompatibility but also mechanical flexibility of the final unit due to physical body movements. To fulfill these requirements polymers have inherent advantage. Polyimide has shown biocompatibility and there are recent works on fabricating micropumps with this material (Komatsuzaki et al. 2011). It also has the disadvantage of curing at high temperatures (around 350°C). For this application, elastomer materials are selected for their stretchability and biocompatibility.

Polydimethylsiloxane (PDMS) is widely used for fabricating microchannels in microfluidics applications (Kim et al. 2008). Some types of this elastomer are biocompatible up to implantation grade (Nusil 2007). One of the developed technologies for fabricating PDMS micro components is soft-lithography in which patterns are transferred from a master mold to PDMS (Kim et al. 2008). Since

A. Jahanshahi (✉)
Department ELIS, Cmst, Ghent University,
Technologiepark 914a, 9052 Ghent, Belgium
e-mail: Amir.Jahanshahi@elis.ugent.be;
Amir.Jahanshahi@imec.be

F. Axisa
Microsys, University of Liege, Liege, Belgium

J. Vanfleteren
Department IMEC, Cmst, Ghent University,
Technologiepark 914a, 9052 Ghent, Belgium

material and fabrication cost for this elastomer are reasonable (Domachuk et al. 2010; McDonald and Whitesides 2002), it is selected as the main processing material. In the literature, there are numerous studies which describe PDMS microchannel fabrication. These microchannels are eventually bonded to a rigid substrate for example silicon (Peterman et al. 2004), or glass (Fadl et al. 2010) to serve as both the carrier and interconnect layer.

In view of fabrication complexity, the electroosmosis micropump features one of the most straightforward and favorable processes among alternative actuation principles, given no need for flow rectification valves (Laser and Santiago 2004). New variants of conventional electroosmosis have emerged in the literature recently (Yang et al. 2009; Mansuripur et al. 2009). Induced charge electroosmosis has been introduced recently (Urbanski et al. 2006). Furthermore, flow over asymmetric electrodes for the first time have been presented (Ajdari 2000; Brown et al. 2000). Topography and charge variation have also been used to induce flow under low DC voltages by Gitlin et al. (2003) and Stroock et al. (2000), respectively. In the topography variation technique, i.e., the adopted transverse electroosmosis phenomena in this work, DC voltages less than 10 V produce flow speeds comparable to high voltages in conventional electroosmosis.

The transverse electroosmosis phenomenon is theoretically introduced and experimentally verified in the literature (Ajdari 2001; Gitlin et al. 2003). The determining factor in the electroosmosis flow (EOF) is the zeta potential. There are reports investigating the PDMS zeta potential in the literature (Tandon et al. 2008). Moreover, it is verified that all PDMS microfluidics, i.e., both microchannel and substrate in PDMS, behave in a similar manner to the usually adopted PDMS-glass structures (Ren et al. 2001). In this contribution all PDMS microchannels are fabricated, however the flow speed characterization is done for a PDMS-glass structure similar to (Gitlin et al. 2003).

For the first time a combination of flexible microfluidics and flexible electronic interconnects is fabricated. This micropump is solely composed of PDMS and gold. For an even better degree of biocompatibility in long-term applications, the same process flow can be used to substitute platinum for gold. In a previous work by this group stretchable gold interconnects using meander shaped conductors with similar 4- μm thick electro-deposited gold layer on top of copper foil is fabricated (Brosteaux et al. 2007). Therefore, in case stretchability in addition to flexibility is needed, the process flow for this unit can be adapted.

2 Design

Transverse EOF is basically the anisotropic response of the fluid to the obliquely angled grooves inside the

microchannel. As shown in Fig. 1, electrodes are placed across the channel on the bottom plane and $\theta = 45^\circ$ oriented grooves are located on top of the microchannel, where h_g , h_c are groove and channel height, and w_g , w_c are groove and channel width, respectively. If the grooves are positioned neither parallel ($\theta = 0^\circ$), nor perpendicular ($\theta = 90^\circ$), there will exist a transversal flow in y direction, proportional to the main flow which is in x and z direction. This flow is called the transverse electroosmosis flow. As schematically depicted in Fig. 1, the micro channel is separated in two parts: the active area with the grooves (l_c) and the microscopy area (l_m). The microscopy area is covered with neither grooves nor electrodes in order to allow observation from the top for micro particle image velocimetry (μ -PIV).

To realize the design with planar thin film and soft lithography processes, two layers of microfluidics and interconnects are separately fabricated, aligned and bonded together. Figure 2 illustrates a schematic diagram of the top and side view of the micropump. The micropump consists of a microfluidics layer and an interconnect layer. The microfluidics layer is composed of the microchannel with liquid reservoirs at its two ends and the grooves. This layer is eventually aligned and bonded to the interconnect layer.

By applying a voltage across the integrated electrodes, a helical flow is formed (Fig. 1) which proves to be useful in active micro mixers (Stroock et al. 2002). Flow speed depends on the applied electrical field, the average surface charge, $(h_g/h_c)^2$ for small (h_g/h_c) ratios, and also on l_m to l_c ratio, where l_c is the channel length. In this work, h_g and h_c are designed 10 and 60 μm , respectively, and w_g of 35 and 70 μm are tested. Tests have shown that, as long as w_g is small compared to w_c , there is no significant importance of this parameter on flow speed.

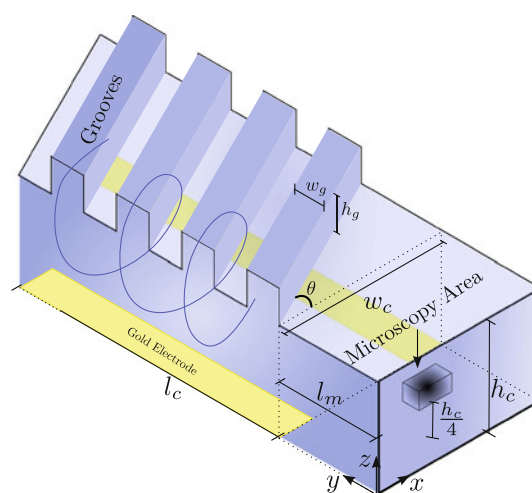


Fig. 1 Schematic diagram of the fabricated electroosmosis pump. The grooves are angled at $\theta = 45^\circ$ along the microchannel (y axis). Electrodes are placed across the microchannel. The helical flow profile is also shown

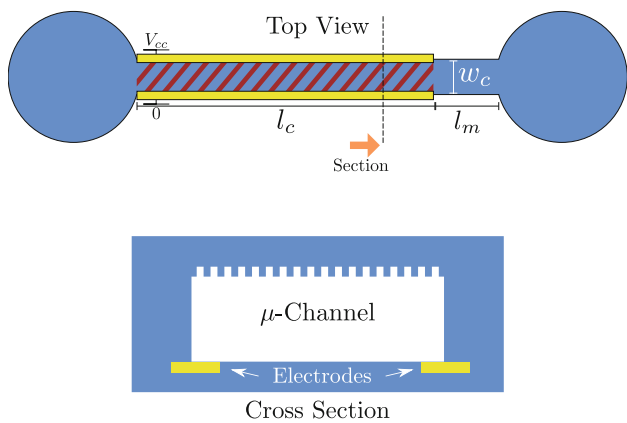


Fig. 2 Micropump design is illustrated in two views. The microfluidics layer consists of a microchannel and grooves. It is aligned and bonded on *top* of the electrical interconnect layer. The dedicated region for microscopy is illustrated (l_m). The *dashed line* shows where the cross section is made

3 Fabrication

In this paper the fabrication process is briefly described and illustrated in Fig. 3. A more detailed fabrication process is reported in a previous work of the authors (Jahanshahi et al. 2011). Fabrication of the interconnect layer is illustrated in different steps in Fig. 3a. It starts off with the standard photolithography patterning of a positive thick photoresist which serves as the mask for a selective electrodeposition of Ni/Au in the next step. An intermediate layer of Ni is electrodeposited prior to Au because of poor adhesion between Au and Cu. This intermediate layer serves also as a barrier for the diffusion of Cu in to Au which is potentially harmful to biocompatibility (Brosteaux et al. 2007). After

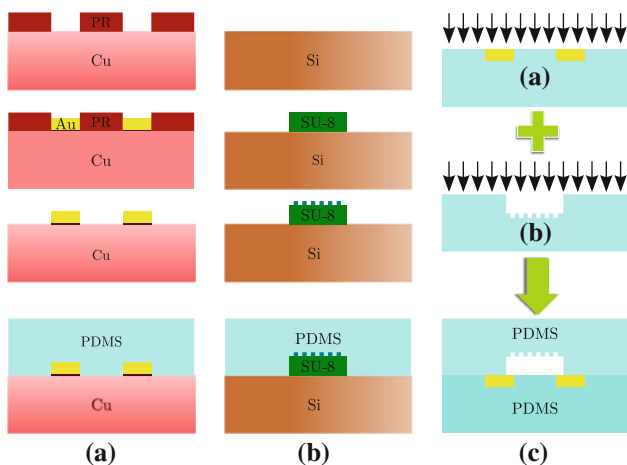


Fig. 3 The process flow of the micropump consists of three major steps. **a** Electrical interconnect layer is fabricated by casting PDMS on Au. **b** Microfluidics layer is fabricated by PDMS soft lithography. **c** Fluidics and interconnect layer are eventually plasma bonded

stripping the resist, Silastic[®] MDX4-4210 biocompatible PDMS from Dow Corning[™] is cast on the wafer and sandwiched between two parallel plates at a pressure of 1 bar to reduce its thickness to 100 μm . MED-6010[®] implantable grade PDMS from Nusil[™] is used also as an alternative for Silastic, since it has a lower viscosity and it is therefore, more convenient to achieve lower thicknesses. After curing the PDMS layer, copper foil and Ni are wet-etched. For speed measurement purposes instead of the fabrication process shown in Fig. 3a, patterned Au on a glass substrate is used as the interconnect layer.

The fabrication process for microfluidics layer is depicted in Fig. 3b. Two layers of SU-8 are patterned sequentially with thicknesses of 60 and 10 μm , in order to form microchannel and grooves mold, respectively. A long pass filter is used to eliminate UV wavelengths below 350 nm during illumination of the SU-8, resulting in sharp vertical edges (Lee et al. 2003). After preparing the mold, PDMS is cast, cured at 70°C for 2 h and subsequently, peeled off. The resulting microfluidics layer, together with the interconnect layer (Fig. 3a) are loaded in a Diener PICO[®] air plasma for 24 s, 0.8 mbar of chamber pressure, and at 190 W power (Fig. 3c). After this surface activation step, both layers are subsequently aligned and bonded together.

The fabrication of the micropump is finalized with the bonding step. The channel and ports should be however hydrophilic in order to be able to pump the liquid, otherwise water would be repelled and the proper function of the pump would be altered. Therefore after 10 min which is sufficient for permanent bonding, the microchannel is filled with DI water to preserve the surface hydrophilicity in the presence of a polar liquid. The later tests have shown that even after 8 months, the channels are hydrophilic and water could be pumped. The preservation of electroosmosis mobility over time is also supported by (Ren et al. 2001). For illustration purposes, a camera image of the final fabricated microfluidics on top of electrodes is illustrated in Fig. 4. The image shows the grooves from the top side along the electrodes across the channel. The onset of the microscopy area is also illustrated.

Concerning the SU-8 multilayer fabrication, solvent evaporation in the UV-exposed regions of the microchannel causes a height variation in the range of few micrometers. Once the second SU-8 layer, i.e., the groove layer, is spin coated, this non-uniformity is transferred also to this layer. This height variation is more severe in the wider channels (Jahanshahi et al. 2011).

4 Results

A camera image of several fabricated micropumps on a PET carrier is illustrated in Fig. 5. From this image, it can be seen that the micro pumps are flexible under severe curving

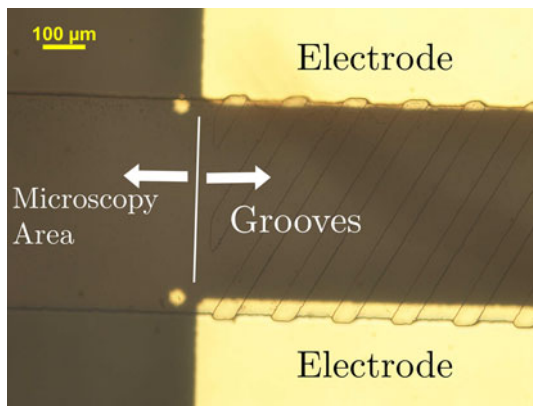


Fig. 4 A camera image of the microfluidics along with electrodes is illustrated. The grooves are located on the *right side* and the microscopy area on the *left*. Groove width is $35\ \mu\text{m}$ and $\theta = 45^\circ$

radius. Three pumps are fabricated together in this sample, and as can be seen batch processing is possible, reducing the total manufacturing and processing costs. The total size of each micropump is $25 \times 1\ \text{mm} \times 400\ \mu\text{m}$ (length \times width \times height). The illustrated sample is merely a prototype and the final product for a specific application can be fabricated substantially smaller in length.

4.1 Confocal laser scanning microscopy

Confocal laser scanning microscopy is a technique for obtaining high-resolution 3D optical images from transparent or complex shaped samples (Pawley 2006). Observing 3D samples using conventional optical microscopes is difficult because of their large depth of field (DoF). In an optical microscope the image is the 2D superposition of all spatial planes of the 3D sample inside the DoF distance. Therefore, the 2D resulting image does not resemble the true 3D object. To overcome this problem confocal microscopes present very fine DoF in order to capture only one spatial plane of the sample in each image. The significance of using confocal microscope in this work

is differentiating between individual micro particles in different spatial planes.

$3\text{-}\mu\text{m}$ dyed amine terminated polystyrene beads from Poly SciencesTM in aqueous solution (2.5% w/v) are diluted 30 times in DI water and are injected into the microchannel as a measure for flow speed. A ZeissTM confocal microscope is used to scan an area of $5\ \mu\text{m}$ height, inside the channel, i.e. the line scan mode with $5\ \mu\text{m}$ DoF. The scan interval is set to $700\ \mu\text{s}$ which is short enough to provide sufficient resolution for the fastest micro particles. Measurements are done on the microscopy area shown in several of the figures in this paper. In this region, there are neither grooves nor electrodes, resulting in no driving force. As a result, the flow profile gradually changes from helical to laminar as the fluid leaves the grooves and sedimentation of micro particles occurs. Because of sedimentation, speed measurements in the middle z -plane is more difficult, especially at lower speeds in which the total number of particles passing the scan line is less. Therefore, the middle plane measurements were only done at 10 and 15 V, in order to have enough particles. For other voltages the measurements were done at $z = h_c/4$ which still had enough particles for measurement purposes.

For illustration purposes two line scan images are shown in Fig. 6. Both images are captured in the microscopy area for a total of 25 s duration, $700\ \mu\text{s}$ sampling rate and over a $17\text{-}\mu\text{m}$ line width. The illustrated images are constructed by stacking the sequential line scans and the red spot shows where a particle was detected. Therefore, a shorter spot height means the particle has passed the scan line faster, i.e., higher flow speed. In Fig. 6a, the micropump is driven with 10 V, while in Fig. 6b, it is driven with 2 V.

4.2 Pumping speed

The substrate was accurately positioned horizontally to minimize the effect of pressure drop due to height difference. After introducing the particles inside the channel and

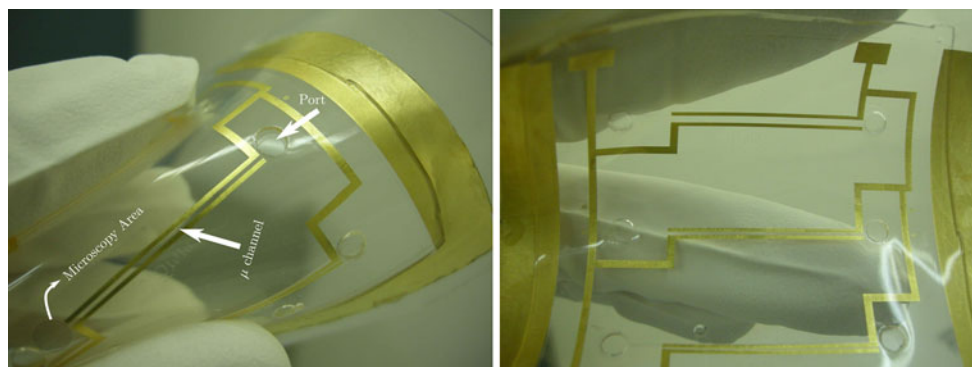


Fig. 5 Camera images showing several micropumps on a PET substrate in different bending conditions. The mechanical flexibility of the sample is visible

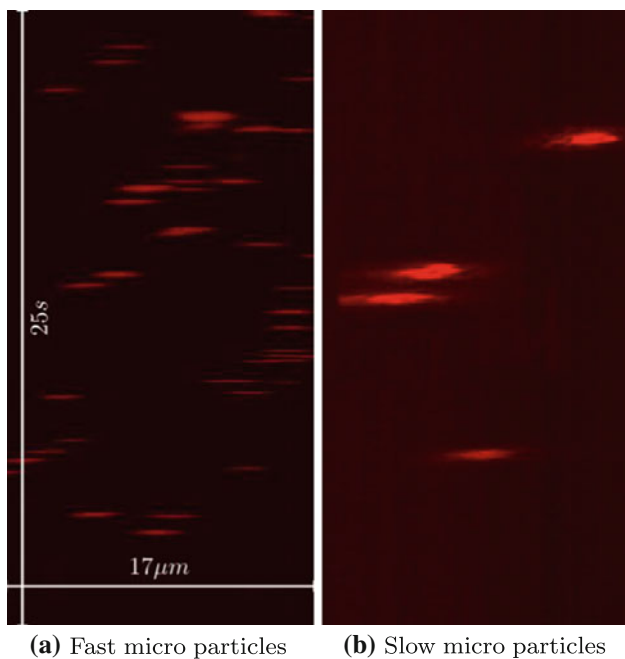


Fig. 6 Two line scan images in the microscopy area are illustrated. In **a** the micropump is driven with 10 V and in **b** it is driven by 2 V. The horizontal axis represents the scan line width, and the vertical axis is the total duration of line scanning

waiting for the pressure drop settlement, measurements were started. Figure 7 illustrates the flow speed of the micropump. A line scan for 60 s duration is performed for each input voltage in the graph. The images are fed to a custom written script which calculates the speed based on the time that it takes for a particle to pass the scan line. The number of particles in the image is from 10 at the lowest speed to 500 at the maximum speed. The speed variation in different micro particles is reflected with the error bars. For better statistical accuracy whenever the number of particles was less than 20, test was redone.

Measurements are done for two different channel widths, 1 mm and 300 µm. There are two major effects that affect the speed. The first one is the electrical field which is relative to the applied voltage and $1/w_c$. Secondly, the pressure drop which is relative to $1/w_c^4$. In wide channels, the former is dominant and as w_c decreases the latter dominates. As can be seen in Fig. 7, flow speed in a 1-mm wide channel is higher compared to a 300-µm wide channel despite higher electrical field. This shows the pressure drop dominance on the flow speed compared to electrical field. Furthermore, the microscopy area located at the end of the microchannel increases the total pressure drop, since there is no driving force in that region. The real speed without the presence of this region would scale up linearly with a factor l_c/l . Figure 7 also shows that for an applied voltage of 10 V over a 1-mm wide channel, speed at $z = h_c/2$ is 1.5

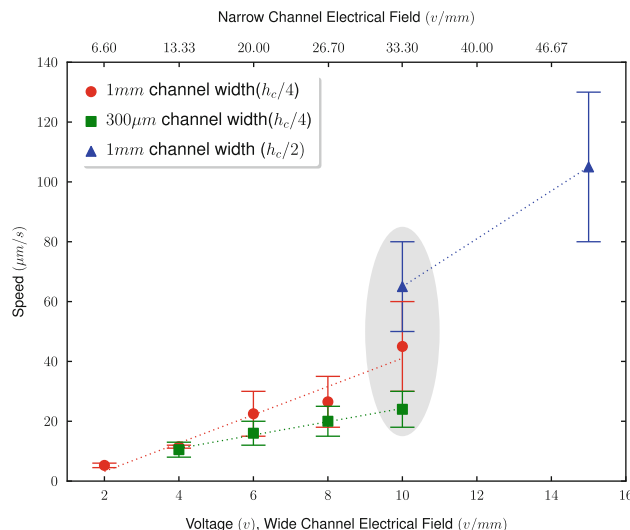


Fig. 7 Flow speed with respect to the applied voltage is shown for channel widths of 1 mm and 300 µm at $z = h_c/4$ spatial plane. Two measurements are also done in the middle plane ($z = h_c/2$) for 10 and 15 V. The electrical field in a wide and narrow channel are illustrated on the bottom and top x axis, respectively. Flow speed at 10 V for three different conditions is highlighted

times higher than speed at $z = h_c/4$ which is a logical observation in the laminar region.

A speed of 60 µm/s at 10 V in the middle plane, yields an average speed of 30 µm/s in a laminar region using the poiseuille equation (e.g. Granger 1985). This results roughly to a flow rate of 1.2 µL/min. This is in accordance to the flow rates reported for commercial drug delivery systems (Evans et al. 2010). Another point of concern for the micropump is water electrolysis, and as a result bubble generation after approximately 5 min of continuous operation. This limits the use of pump in continuous mode operation. Back-pressure of the pump is not measured explicitly, although it is expected to be in the range of 10 Pa which is relatively low.

4.3 Mechanical flexibility

There are mainly two factors contributing to crack formation: the gold thickness and conductor track width. As the width scales down gold becomes more stretchable and therefore, cracks are formed at higher elongations. Nevertheless, there is a tradeoff between track width, or more generally surface area, and the layer conductivity. Experimentally under the condition of 2-cm curving radius, the 2-µm thick and 200-µm wide tracks did not show any visible crack.

In Fig. 8, two gold layers embedded in PDMS are illustrated. In Fig. 8a, the thickness is 100 nm and cracks are formed mostly in large surface area structures. In Fig. 8b the gold thickness is 5 µm, and despite the large

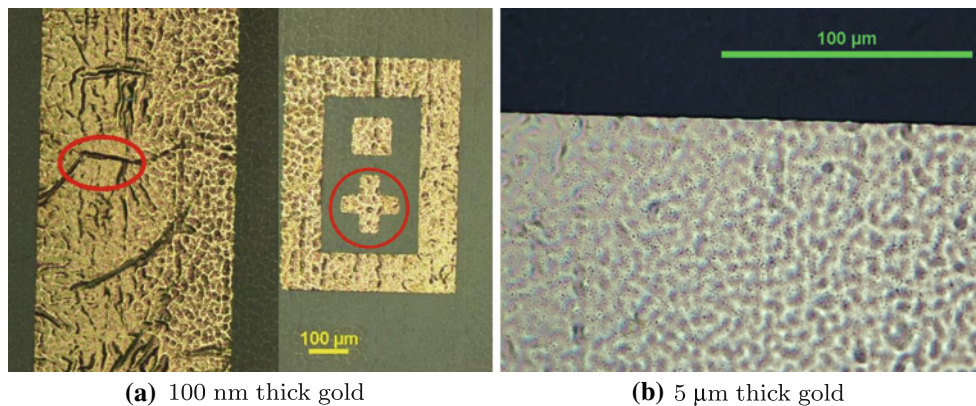


Fig. 8 **a** Cracks in the wide track on the *left* are visible. Crack formation dependence on the total surface area is presented in this figure. **b** Despite the track width, there is no visible crack. The rough surface of Au and PDMS is due to the commercial Cu-foil surface roughness

surface area there is no visible crack. The rough surface of gold and PDMS is due to the sacrificial Cu-foil surface roughness, even though the processing is done on the smooth side of the foil.

5 Conclusion and future work

In this work, a flexible electroosmosis micropump is demonstrated and fabricated using the presented flexible interconnection technology. It is composed of only biocompatible PDMS elastomer and a thin layer of gold which is embedded in PDMS. While keeping high biocompatibility degrees, it also features flexibility even at high bending curvatures. The fabrication process can even be adapted to our previously reported stretchable interconnect technology (Brosteaux et al. 2007) to produce stretchable micropumps. The micropump flow speed is characterized using line scanning technique with a confocal microscope. It features a flow speed of $60 \mu\text{m/s}$ at relatively low DC voltage of 10 V. Therefore, it is particularly useful in battery powered and hand-held devices not capable of holding large power supplies and not needing a full time operation.

Concerning the mechanical performance, better results can be achieved by supporting the gold interconnects with a flexible polymer such as polyimide and also by shaping them in meander form. Once a flexible polymer supports the gold meanders, fatigue is heavily improved (Hsu et al. 2011). This work is now under progress by the authors.

The most notable drawback is the relatively low maximum back pressure of 10 Pa. The authors believe that with careful design control and proper positioning of input and output reservoirs in a loop or circle such as a spiral structure with minimum height difference, this issue can be overcome to a great extent. Furthermore, to preserve the micro channel hydrophilicity, it should be always in

contact with a polar solution. Therefore this micropump is inappropriate for pumping non polar solutions.

The other drawback is that the flow rate is dependent on the working liquid. As the ionic concentration of the solution is increased, the flow rate decreases. Therefore, the pumping feasibility should be verified in a specific application with a specific fluid. Another concern is the bubble generation after 5 min of continuous operation due to water electrolysis. Therefore, using solutions with less ionic concentration is preferred. The flow rate variation with respect to working liquid, and bubble generation are however drawbacks applicable to all kinds of electroosmosis and electrokinetic driven micropumps.

Acknowledgments This work is granted through an IMEC PhD scholarship. The authors would like to express their gratitude to Dr. Chengxun Liu and Dr. Tim Stakenborg for their kind assistance in confocal microscopy measurements at IMEC, Leuven. The authors acknowledge Sheila Dunphy for her support.

References

- Ajdari A (2000) Pumping liquids using asymmetric electrode arrays. *Phys Rev E* 61(1):R45–R48. doi:[10.1103/PhysRevE.61.R45](https://doi.org/10.1103/PhysRevE.61.R45)
- Ajdari A (2001) Transverse electrokinetic and microfluidic effects in micropatterned channels: lubrication analysis for slab geometries. *Phys Rev E* 65(1):016301. doi:[10.1103/PhysRevE.65.016301](https://doi.org/10.1103/PhysRevE.65.016301)
- Amirouche F, Zhou Y, Johnson T (2009) Current micropump technologies and their biomedical applications. *Microsyst Technol* 15:647–666. doi:[10.1007/s00542-009-0804-7](https://doi.org/10.1007/s00542-009-0804-7)
- Brosteaux D, Axisa F, Gonzalez M, Vanfleteren J (2007) Design and fabrication of elastic interconnections for stretchable electronic circuits. *IEEE Electron Device Lett* 28(7):552–554. doi:[10.1109/LED.2007.897887](https://doi.org/10.1109/LED.2007.897887)
- Brown ABD, Smith CG, Rennie AR (2000) Pumping of water with ac electric fields applied to asymmetric pairs of microelectrodes. *Phys Rev E* 63(1):016305. doi:[10.1103/PhysRevE.63.016305](https://doi.org/10.1103/PhysRevE.63.016305)
- Chung AJ, Kim D, Erickson D (2008) Electrokinetic microfluidic devices for rapid, low power drug delivery in autonomous microsystems. *Lab Chip* 8:330–338. doi:[10.1039/B713325A](https://doi.org/10.1039/B713325A)

- Domachuk P, Tsioris K, Omenetto FG, Kaplan DL (2010) Biomicrofluidics: biomaterials and biomimetic designs. *Adv Mater* 22(2):249–260. doi:10.1002/adma.200900821
- Evans A, Park J, Chiravuri S, Gianchandani Y (2010) A low power, microvalve regulated architecture for drug delivery systems. *Biomed Microdevice* 12:159–168. doi:10.1007/s10544-009-9372-y
- Fadl A, Demming S, Zhang Z, Bnttgenbach S, Krafczyk M, Meyer D (2010) A multifunction and bidirectional valve-less rectification micropump based on bifurcation geometry. *Microfluid Nanofluid* 9:267–280. doi:10.1007/s10404-009-0544-0
- Feng GH, Kim ES (2004) Micropump based on pzt unimorph and one-way parylene valves. *J Micromech Microeng* 14(4):429. <http://stacks.iop.org/0960-1317/14/i=4/a=001>
- Gitlin I, Stroock AD, Whitesides GM, Ajdari A (2003) Pumping based on transverse electrokinetic effects. *Appl Phys Lett* 83(7):1486–1488. doi:10.1063/1.1602560
- Granger R (1985) *Fluid mechanics*. Holt, Rinehart, and Winston. <http://books.google.com/books?id=06fAL6bxLBIC>
- Hsu YY, Gonzalez M, Bossuyt F, Axisa F, Vanfleteren J, Wolf ID (2011) The effects of encapsulation on deformation behavior and failure mechanisms of stretchable interconnects. *Thin Solid Films* 519(7):2225 – 2234. doi:10.1016/j.tsf.2010.10.069, <http://www.sciencedirect.com/science/article/B6TW0-51DD91W-1/2/2102575280202db0e562eeae1746d08>
- Jahanshahi A, Axisa F, Vanfleteren J (2011) Fabrication of an implantable stretchable electro-osmosis pump. *SPIE*, vol 7929, p 79290R. doi:10.1117/12.873812, <http://link.aip.org/link/?PSI/7929/79290R/1>
- Jeong OC, Park SW, Yang SS, Pak JJ (2005) Fabrication of a peristaltic pdms micropump. *Sensors Actuators A: Phys* 123-124:453–458. *Eurosensors XVIII 2004—The 18th European conference on Solid-State Transducers*. doi:10.1016/j.sna.2005.01.035, <http://www.sciencedirect.com/science/article/B6THG-4FJKWT4-5/2/7ae7ae8897f9b40e8113e4daf6e4401d>
- Kim JH, Na KH, Kang C, Kim YS (2005) A disposable thermopneumatic-actuated micropump stacked with pdms layers and ito-coated glass. *Sensors Actuators A: Phys* 120(2):365–369. doi:10.1016/j.sna.2004.12.024, <http://www.sciencedirect.com/science/article/B6THG-4FBW5XR-1/2/12b41e0ce8de4872d5703838705024d7>
- Kim P, Kwon KW, Park MC, Lee SH, Kim SM, Suh KY (2008) Soft lithography for microfluidics: a review. *Biochip J* 2(1):1–11
- Komatsuzaki H, Suzuki K, Liu Y, Kosugi T, Ikoma R, Youn SW, Takahashi M, Maeda R, Nishioka Y (2011) Flexible polyimide micropump fabricated using hot embossing. *Jpn J Appl Phys* 50(6):06GM09. doi:10.1143/JJAP.50.06GM09
- Laser DJ, Santiago JG (2004) A review of micropumps. *J Micromech Microeng* 14(6):R35. <http://stacks.iop.org/0960-1317/14/i=6/a=R01>
- Lee S, Shi W, Maciel P, Cha S (2003) Top-edge profile control for su-8 structural photoresist. In: *Proceedings of the 15th Biennial. University/Government/Industry Microelectronics Symposium, 2003*, pp 389–390. doi:10.1109/UGIM.2003.1225777
- van Lintel H, van De Pol F, Bouwstra S (1988) A piezoelectric micropump based on micromachining of silicon. *Sensors Actuators* 15(2):153–167. doi:10.1016/0250-6874(88)87005-7, <http://www.sciencedirect.com/science/article/B6W97-44W5JV0-FW/2/d659058f9bcb83c80de10e5f4cc03c34>
- Mansuripur TS, Pascall AJ, Squires TM (2009) Asymmetric flows over symmetric surfaces: capacitive coupling in induced-charge electro-osmosis. *New J Phys* 11(7):075030. <http://stacks.iop.org/1367-2630/11/i=7/a=075030>
- McDonald JC, Whitesides GM (2002) Poly(dimethylsiloxane) as a material for fabricating microfluidic devices. *Accounts of Chemical Research* 35(7):491–499. doi:10.1021/ar011010q, <http://pubs.acs.org/>
- Nusil (2007) Med-6010. <http://www.silicone-polymers.co.uk/pdf2007/MED-6010P.pdf>
- Pawley J (2006) *Handbook of biological confocal microscopy*. Springer, Berlin
- Peterman MC, Noolandi J, Blumenkranz MS, Fishman HA (2004) Localized chemical release from an artificial synapse chip. *Proceedings of the National Academy of Sciences of the United States of America* 101(27):9951–9954. doi:10.1073/pnas.0402089101, <http://www.pnas.org/content/101/27/9951.abstract>, <http://www.pnas.org/content/101/27/9951.full.pdf+html>
- Ren X, Bachman M, Sims C, Li G, Allbritton N (2001) Electroosmotic properties of microfluidic channels composed of poly(dimethylsiloxane). *Journal of Chromatography B: Biomedical Sciences and Applications* 762(2):117–125. doi:10.1016/S0378-4347(01)00327-9, <http://www.sciencedirect.com/science/article/>
- Stroock AD, Weck M, Chiu DT, Huck WTS, Kenis PJA, Ismagilov RF, Whitesides GM (2000) Patterning electro-osmotic flow with patterned surface charge. *Phys Rev Lett* 84(15):3314–3317. doi:10.1103/PhysRevLett.84.3314
- Stroock AD, Dertinger SKW, Ajdari A, Mezic I, Stone HA, Whitesides GM (2002) Chaotic Mixer for Microchannels. *Science* 295(5555):647–651. doi:10.1126/science.1066238, <http://www.sciencemag.org/cgi/content/abstract/295/5555/647>, <http://www.sciencemag.org/cgi/reprint/295/5555/647.pdf>
- Tandon V, Bhagavatula SK, Nelson WC, Kirby BJ (2008) Zeta potential and electroosmotic mobility in microfluidic devices fabricated from hydrophobic polymers: 1. the origins of charge. *Electrophoresis* 29(5):1092–1101. doi:10.1002/elps.200700734
- Urbanski JP, Thorsen T, Levitan JA, Bazant MZ (2006) Fast ac electro-osmotic micropumps with nonplanar electrodes. *Appl Phys Lett* 89(14):143508. doi:10.1063/1.2358823, <http://link.aip.org/link/?APL/89/143508/1>
- Yang H, Jiang H, Ramos A, García-Sánchez P (2009) Ac electrokinetic pumping on symmetric electrode arrays. *Microfluidics and Nanofluidics* 7:767–772. doi:10.1007/s10404-009-0434-5
- Zengerle R, Kluge S, Richter M, Richter A (1995) A bidirectional silicon micropump. 19. doi:10.1109/MEMSYS.1995.472560